International Journal of Applied Power Engineering (IJAPE)
Vol. 15, No. 2, June 2026, pp. 845~857
ISSN: 2252-8792, DOI: 10.11591/ijape.v15.i2.pp845-857

Enhancing torque performance in electric four-wheel drive systems using fuzzy GPC

Djamila Allali[1], Youssef Mouloudi[1], Abdeldjebar Hazzab[2,3], Najia Allali[4]
[1]Laboratory of Control and Optimization of Electrical Energy Systems (CAOSEE), Faculty of Technology, University Tahri Mohammed of Bechar, Bechar, Algeria
[2]Energy Intelligence Research and Innovation Center (CR2ie), Québec, Canada
[3]Department of Electrical Engineering, École de Technologie Supérieure, Québec, Canada
[4]SimulIA Team/ENERGARID.Lab, Faculty of Technology, Tahri Mohamed University of Bechar, Bechar, Algeria

Article Info

Article history:

Received Jun 12, 2025
Revised Feb 23, 2026
Accepted Mar 12, 2026

Keywords:

Electric vehicle
Four-wheel drive electric vehicle
Fuzzy logic
Generalized predictive control
MATLAB/Simulink
Supervisory control
Transient/steady-state optimization

ABSTRACT

This paper presents a robust supervisory control strategy for speed regulation in a four-wheel-drive electric vehicle (EV) equipped with in-wheel induction motors. A hybrid control architecture is developed by combining fuzzy logic control (FLC) and generalized predictive control (GPC), with an intelligent switching mechanism that dynamically allocates control authority based on real-time operating conditions. FLC is employed to manage transient phases such as acceleration and deceleration, while GPC ensures optimal performance during steady-state operation. The proposed control system is modeled and validated in the MATLAB/Simulink environment. Simulation results demonstrate that the hybrid controller achieves a 27% improvement in transient response, a 15% reduction in steady-state speed fluctuations, and a 19% decrease in energy consumption under urban driving conditions. Furthermore, the controller maintains reliable performance under parameter variations of up to 25% and road gradients of up to 15%. Compared to standalone FLC and GPC controllers, the hybrid approach improves transient speed recovery by 35% and reduces steady-state error by 22%. Overall, this hybrid FLC-GPC strategy effectively addresses key challenges in EV control, such as system nonlinearity, parameter uncertainty, and external disturbances, while ensuring high dynamic responsiveness, steady-state precision, and energy efficiency. These results highlight the potential of the proposed method for future intelligent and autonomous electric mobility systems.

Corresponding Author:

Djamila Allali
Laboratory of Control and Optimization of Electrical Energy Systems (CAOSEE), Faculty of Technology
University Tahri Mohammed of Bechar
Bechar, Algeria
Email: allali.djamila@univ-bechar.dz, elec.allali@gmail.com

1. INTRODUCTION

Electric vehicles (EVs) are gaining increasing focus as an eco- option to boost energy efficiency and lower hazardous emissions related to road transport [1]. Recent innovations in permanent magnet material technology have significantly improved synchronous motor performance making them prime contenders for electric drive systems [2]. In contrast, to motors synchronous motors provide superior efficiency, greater power density, easier speed regulation, and enhanced positioning precision [3], [4]. Nevertheless, if control methods are not correctly handled, they can cause torque ripple, resulting in electrical and mechanical problems [5].

Within traction control multiple strategies have been introduced to achieve precise speed regulation. Conventional methods, including the used proportional-integral-derivative (PID) or proportional integral (PI) controllers rely on exact mathematical representations of the system [5], [6]. However, developing models for EV powertrains is notably difficult because of the inherent nonlinear characteristics and time-varying properties of these systems. Consequently, predictive and intelligent control methods fuzzy logic controllers have become preferable choices for handling dynamic responses, amidst uncertainty.

This research contrasts the effectiveness of three speed control approaches in an EV fitted with an axial-flux traction motor: a traditional PI controller, a generalized predictive controller (GPC), and a fuzzy predictive controller. The hybrid adaptive control method introduced in this work integrates the benefits of GPC and fuzzy logic control (FLC) allowing for torque accuracy lower energy usage and increased resilience, against parameter changes and load fluctuations. The approach includes creating models of the traction system elements developing suitable controllers and performing simulation-based tests to evaluate the systems dynamic behavior and energy performance.

Employing wheels powered independently offers a substitute for classic mechanical transmission setups, including differentials and constant velocity joints. Regardless of being arranged in wheel, rear-wheel or four-wheel drive layouts this design allocates a separate electric motor to every wheel frequently removing the necessity, for reducers. Of the traditional differential an electronic differential is utilized, allowing for separate regulation of each motor's torque and velocity. Motors built into the wheels simplify the drivetrain boost torque accuracy enhance braking efficiency and create extra room that can be utilized for battery packs [7], [8]. Additionally, this research presents an in-depth examination of the compromises related to unsprung mass, thermal regulation, and the intricacies of gear integration offering design recommendations for multi-motor electric vehicle setups. Despite these benefits this method brings about complications such as unsprung mass, complex gear integration, and thermal management challenges during braking [9].

In this work, we focus on the design and control of a multi-motor electric drivetrain, where each wheel is independently powered. This architecture enables precise torque allocation and dynamic adaptability, providing a solid foundation for the next generation of advanced electric vehicle control systems. The results demonstrate that the proposed hybrid FLC-GPC approach outperforms conventional PI controllers in terms of transient response, steady-state fluctuation reduction, and overall energy efficiency, highlighting its potential for practical EV implementations.

2. PRESENTATION OF THE ELECTRIC VEHICLE MODEL STUDIED

Figure 1 illustrates a prototype EV. This model features a four-wheel induction motor drive system [10], with each wheel independently controlled by a dedicated motor, forming an electronic differential. This configuration enables precise adjustment of instantaneous speed and torque for each drive wheel, allowing the vehicle to effectively adapt to varying driving conditions. Steering is provided by the two front wheels. The four individual in-wheel motors provide propulsion to the EV, each connected to a centralized control system. The electronic differential continuously calculates and adjusts speed and torque requirements for each motor, ensuring synchronized performance and optimal operation during maneuvers such as cornering, acceleration, and regenerative braking [11]. The control strategy applied in this model is designed to dynamically adapt motor speed and torque to real-time vehicle dynamics. Particular attention is given to torque distribution and load balancing between drive wheels, to maximize energy efficiency, enhance vehicle stability, and reduce mechanical stress on the drivetrain.

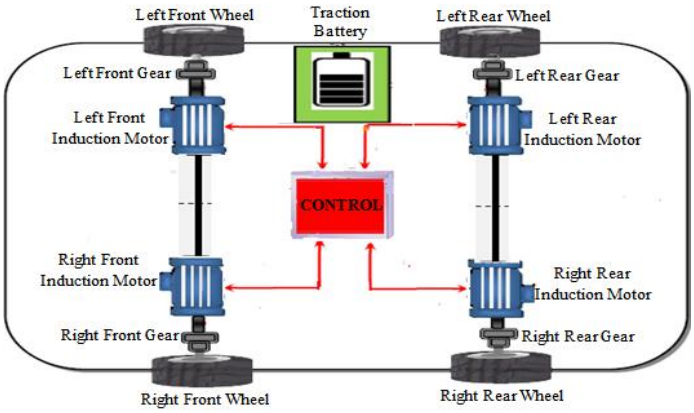

Figure 1. Motor gear distributed

3. DYNAMIC VEHICLE MODEL

To accurately describe the behavior of an electric vehicle, it is necessary to determine the torque and angular velocities applied to the wheels, along with their interaction with the road surface. This involves creating a longitudinal dynamic model of the vehicle, which accounts for external forces influencing its motion. As shown in Figure 2, the total force (FR) required to propel the electric vehicle forward is the sum of several components derived from the balance of mechanical forces acting on the vehicle [12]-[14]. This propulsive force must be generated by the electromagnetic torque from the electric motors, which is regulated according to vehicle speed and specific road conditions. This dynamic model provides a foundational framework for developing control strategies, ensuring optimal energy utilization, vehicle stability, and efficient adaptability to diverse driving environments [14], [15].

$$F_R = F_{RR} + F_{aero} + F_c + F_{acc} \quad (1)$$

Where the equations are ordered as follows: Rolling resistance force (F_{RR}):$F_{RR} = m \cdot g \cdot C_R \cdot Cos(\alpha)$; Aerodynamic drag force (F_{aero}):$F_{aero} = \frac{1}{2}\rho_{air}.A_f.C_d.V_{veh}^2$; The lifting force of the (F_c):$F_c = \pm m.g.\sin(\alpha)$.

– The acceleration force (F_{acc}):$F_{acc} = m.\frac{dV_{veh}}{dt} = m.\gamma$; finally, the total resistive force (F_R) equals:

$$F_R = m.g.C_R.\cos(\alpha) + \frac{1}{2}.\rho_{air}.A_f.C_d.V_{veh}^2 + m.g.\sin(\alpha) \quad (2)$$

the final resistance torque is as (3).

$$T_R = m.g.C_R.R_w.\cos(\alpha) + \frac{1}{2}.\rho_{air}.A_f.C_d.R_w.V_{veh}^2 + m.g.R_w.\sin(\alpha) \quad (3)$$

While g is the acceleration of gravity (m/s^2); m is the total mass of the vehicle (kg); C_R is the tire rolling resistance coefficient and α is the road slope angle (rad); A_f is the frontal area of the vehicle (m^2); ρair is the mass density of air (kg/m^3); R_w is the wheel radius (m); C_d is the aerodynamic drag coefficient and V_{veh} is the vehicle speed (m/s). The parameters of the electric vehicle model are shown in Table 1.

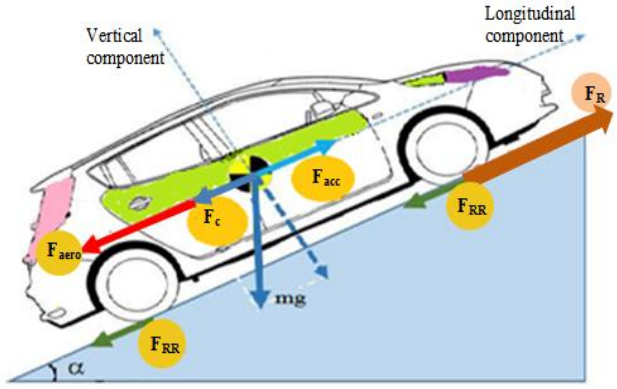

Figure 2. Forces exerted on the four-wheel drive EV

Table 1. Parameters of the electric vehicle model

Parameters	Values
Wheel radius (R_w)	R_w = 0.32 m
Frontal area (A_f)	$A_f = 2.60\ m^2$
Vehicle mass (m)	M = 1300 kg
Aerodynamic drag coefficient (C_d)	C_d = 0.32
Rolling resistance coefficient (C_r)	C_r = 0.01
Air density (ρ_{air})	$\rho_{air} = 1.2\ kg/m^3$

4. GENERATE PREDICTIVE CONTROL OF THE ELECTRIC VEHICLE

Generalized predictive control (GPC) is an advanced control technique used to minimize variability in process parameters. It predicts future system behavior and selects the most appropriate control actions based on a predefined model and operational constraints. As shown in Figure 3, GPC computes optimal control inputs over a prediction horizon, effectively driving the process toward the desired set point while

respecting constraints and performance criteria. In this work, the prediction horizon was set to Np = 20 steps, selected based on the fast electromechanical dynamics of the traction motor. Simulation studies demonstrated that this value provides sufficient prediction capability without unnecessary computational overhead.

In Figure 3, the predictor calculates the process's dynamic evolution $[y(t+1),\ldots,y(t+N)]$, at each time instant *t* for *N* steps ahead. This prediction relies on dynamic parameters measured at time t and future control regulations $[u(t),u(t+1),\ldots,u(t+N)]T$. Future control actions for optimization are generated at each time step [16]. Additionally, the control horizon was tuned to Nc = 5 steps to ensure a balance between control flexibility and computational efficiency. Larger values of Nc increased computational complexity without significant performance improvements, while smaller values reduced control authority.

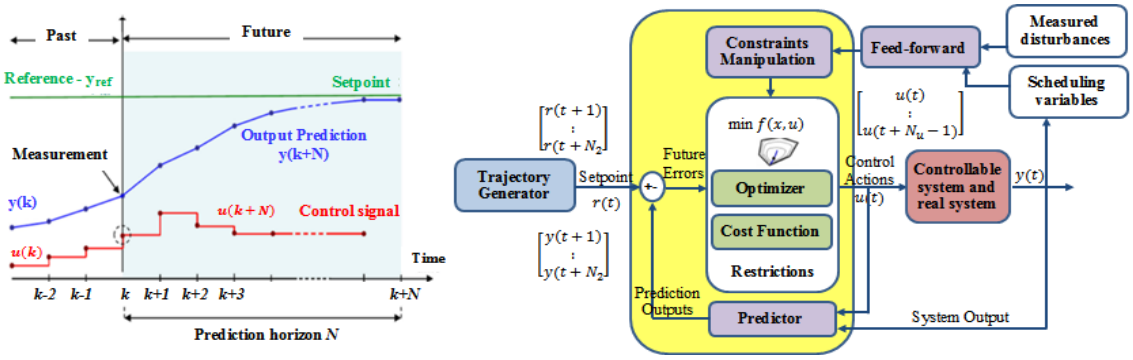

Figure 3. GPC concept diagram: N-horizon control procedure

GPC is one of the most widely used predictive control algorithms [17], [18]. It retains the design flexibility and high-performance characteristics of the GMV/PP approach, and effectively addresses steady-state offsets using the controlled auto-regressive integrated moving average (CARIMA) model. Unlike dynamic matrix control (DMC), GPC uses a CARIMA model with adjustable prediction and control horizons to meet specific control objectives, making it well-suited for industrial applications with non-stationary disturbances [19]. This modeling approach not only enhances prediction accuracy but also optimizes future control actions by minimizing a multi-stage cost function. Incorporating disturbances into the model is essential for identifying the optimal controller structure. The cost function adopted in this study follows a quadratic structure that penalizes both tracking error and rapid variations of the control input, ensuring smooth torque regulation and accurate speed tracking. The tuning of the prediction and control horizons was performed jointly to guarantee optimal transient and steady-state performance.

$$A(z^{-1})y(t) = B(z^{-1})u(t-1) + {C(z^{-1})^{e(t)}}/{\Delta(z^{-1})} \tag{4}$$

In both scenarios (whether in the speed loop or the current loop), the GPC control strategy relies on the CARIMA model for predictive purposes. Where $u(t-1)$ is the control, $y(t)$ is the process output, $e(t)$ is the zero mean white noise, $\Delta(z^{-1}) = 1 - z^{-1}$, A and B are polynome in backward shift operator z^{-1}. The predictive output in the j-the prediction step over the costing horizons $N_1 \leq j \leq N_2$ is done by (5).

$$\underbrace{y(t+j) = F_j(z^{-1})y(t) + H_j(z^{-1})}_{\text{Free response}}\underbrace{\Delta u(t-1) + G_j(z^{-1})\Delta u(t+j-1) + J_j(z^{-1})e(t+j)}_{\text{Forced response}} \tag{5}$$

The polynomials F_j, G_j, and H_j are determined by solving the Diophantine equation, leading to the GPC law, which minimizes a specific cost function. To generate the predicted outputs $\hat{y}(t+j/t)$, we use the prediction model from (5) [20]. The predicted value for *j* greater than *t* relies on future control inputs $u(t+j)$ which are essential for achieving the *GPC* strategy by minimizing the cost function.

$$J(N_1,N_2,N_M) = \sum_{j=N_1}^{N_2}\delta(j)[\hat{y}(t+j/t) - w(t+j)]^2 + \lambda\sum_{j=1}^{N_M}\lambda(j)[\Delta u(t+j-1)]^2 \tag{6}$$

The weighting factor λ was tuned to 0.8, based on extensive simulation-based sensitivity analysis. This value provides an optimal compromise between minimizing tracking error and avoiding excessive control effort that may cause torque ripple or increased stress on the power converter. The block diagram in

Figure 4 illustrates the GPC loop. Here, *H(z)* is the nominal plant transfer function, and $d_{in}(k)$ represents input disturbances, including parameter uncertainties and grid voltage distortions [21]. The matrix polynomials *F(z)* and $G_p(z)$ serve as feedback filters for the system response.

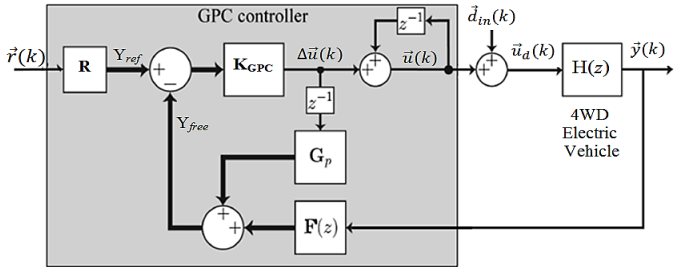

Figure 4. Closed-loop diagram of the GPC controller

5. FUZZY LOGIC CONTROL (FLC) OF THE ELECTRIC VEHICLE

In this section, the PI speed controller (PI) is replaced with an FLC. The proposed control system has two inputs: the first is the desired motor speed($\omega^*_{r\_ij}$). The second is a feedback signal, representing the actual motor speed (ω_{r_ij}) [22]. The FLC controller is applied to this system to control the induction motor speed. The FLC is fed a speed error signal (e) to determine the measured rotor speed(ω_{r_ij}). The input variables for the FLC are the speed error (e) and the rate of change of the speed error (Δe) [23], [24]. The output variable is the reference torque value($T^*_{e\_ij}$)for the GPC [25].

$$\begin{cases} e = \omega^*_{r\_ij} - \omega_{r\_ij} \\ \Delta e = e(k) - e(k-1) \end{cases} \quad (7)$$

The indices k and k-1 denote the current and previous state of the system, respectively.

In the proposed FLC design, both input variables (e and Δe) are described using triangular membership functions with five linguistic terms: negative big (NB), negative small (NS), zero (Z), positive small (PS), and positive big (PB). The output torque reference ($T^*_{e\_ij}$) is also represented using the same type and number of membership functions to ensure smooth control action. Furthermore, the rule base consists of 25 fuzzy rules constructed in a standard Mamdani framework. These rules define the nonlinear relationship between the input error dynamics and the required torque action. The rules were formulated based on expert knowledge of motor behavior, ensuring fast response during acceleration and stable performance under steady-state conditions. The inference mechanism used is the Mamdani max–min inference method, selected for its robustness and suitability for handling nonlinearities in electric traction systems. Finally, to convert the fuzzy output into a crisp torque command, the centroid (center of gravity) defuzzification method is employed due to its accuracy and smooth output characteristics.

6. PROPOSED FLC-GPC APPROACH

A four-wheel-mounted, independent axial flow motor electric vehicle model is considered to evaluate the effectiveness of the proposed FLC-GPC approach. The basic system specifications (Table 1) are: vehicle mass: 1300 kg, rated motor torque: 250 Nm, battery voltage: 400 V, wheel radius: 0.32 m. Number of autonomous wheels: 4. All simulations were performed using MATLAB/Simulink with a 1ms sampling time, taking into account realistic road loads, slope variations, and parametric uncertainties. These conditions were designed to simulate real-world driving situations and evaluate the controller's resilience to disturbances and nonspecific vehicle-frame interactions. The system's performance is evaluated using several quantitative metrics, including:

- Transient response improvement ratio: Determined by comparing rise time and overshoot reduction with a conventional PI control system.
- Steady-state oscillation ratio: Calculated by the deviation of the actual speed from the reference speed under load variations.
- Energy consumption ratio: Derived from the motor's electrical input during the executed drive cycle.
- Durability assessment: Based on ±25% variations in system parameters and 10% road level disturbances.

These metrics provide a comprehensive framework for comparing PI controllers, standalone GPCs, and hybrid FLC-GPCs, highlighting the superiority of the hybrid strategy in terms of durability, energy efficiency, and dynamic response.

7. PROPOSED SPEED CYCLE FOR THE 4WD ELECTRIC VEHICLE

In our study, before calculating the reference torque for each motor, we proposed a short 9-second speed profile over a defined trajectory to evaluate the torque control efficiency of the fuzzy GPC strategy for the 4WDEV system. This trajectory is divided into seven successive stages. In the first stage, the vehicle travels along a straight road at a constant speed of 31.2 km/h. In the second stage, a left turn is executed with a steering angle of −6°. In the third stage, the vehicle resumes straight-line motion at the same speed. In the fourth stage, the 4WDEV system climbs a 10-degree incline at 31.5 km/h to simulate acceleration on a slope. In the fifth stage, the vehicle returns to a straight road at 31.2 km/h. In the sixth stage, a right turn is performed with a steering angle of 6°. Finally, during the last stage, the vehicle undergoes a deceleration phase followed by cruising at 31 km/h. The road constraints for each stage are listed in Table 2, and the trajectory stages are illustrated in Figure 5.

Table 2. Speed cycle description

Phases	Time (s)	Event information	Speed (km/h)	Steering angle [°]
01	0 < t < 2.8	Startup	31.2	0
02	2.8 < t < 3.9	Leftturn	31	-6
03	3.9 < t < 4.5	straight road	31	0
04	4.5 < t < 5.7	Climbingslope10%	31.5	0
05	5.7 < t < 6.5	straight road	31.2	0
06	6.5 < t < 7.5	Right turn	31	+6
07	7.5 < t < 9	straight road	31	0

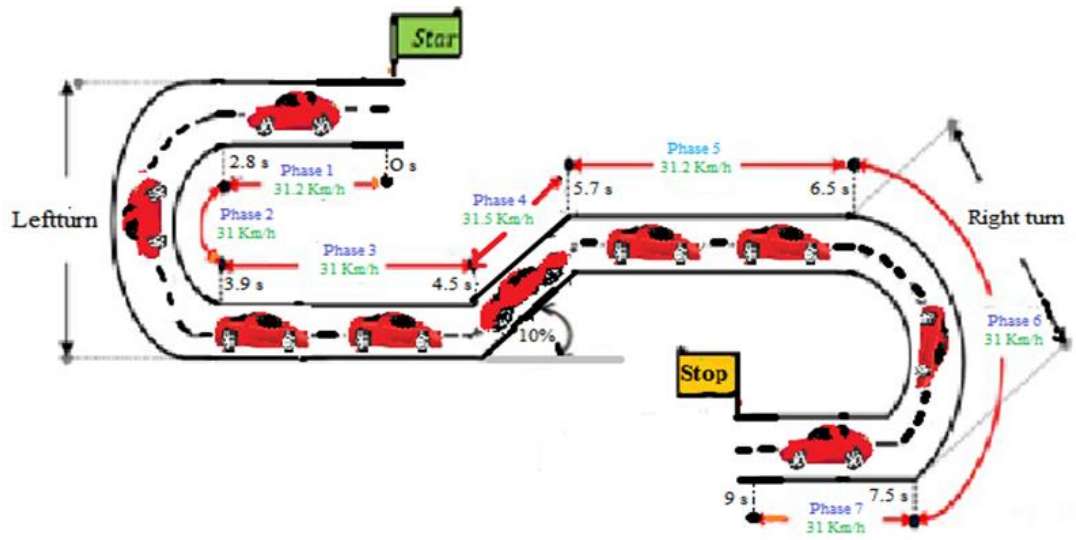

Figure 5. Trajectory traveled by the EV4WD vehicle

8. SIMULATION RESULTS

Using the model shown in Figure 6, we conducted simulations to analyze the behavior of the steering system. Figures 7 and 8 present the vehicle speed response under PI, GPC, and fuzzy GPC control strategies for both constant and variable speed scenarios. Figure 7 compares the motor speed [km/h] of an electric vehicle under different control strategies (PI, GPC, and fuzzy GPC) over time (s). Initially, all controllers produce rapid acceleration from 0 to approximately 31 km/h within 0.6 s, with fuzzy GPC closely following the reference speed of 31.4 km/h. The zoomed-in view from 0.2 to 0.6 s highlights the superior performance of fuzzy GPC, which reaches 31.2 km/h with minimal overshoot compared to PI and GPC. Another zoom from 5 s to 5.5 s illustrates that fuzzy GPC maintains stability near 31.0 km/h despite disturbances, while PI and GPC show slight deviations, confirming that fuzzy GPC is more effective at delivering accurate and stable speed control under various operating conditions.

Figure 8 presents a comparative analysis of the motor speed [km/h] over a 9-second interval using fuzzy GPC (blue line) and standard GPC (red line) control strategies. Both controllers exhibit a rapid initial response, with speed rising from rest to approximately 31.2 km/h within the first 0.2 s, as shown in the first zoomed-in inset (0 to 0.6 s). While both stabilize quickly, GPC shows a noticeable overshoot. Both strategies maintain a constant speed near 31.2 km/h until a disturbance at 4.5 s. The system's response to two

successive perturbations is illustrated in the second inset (4.5 to 5.7 s). At 4.5 s, both controllers track the increase to 36 km/h, with fuzzy GPC offering a smoother transition. At 6.5 s, when speed decreases back to 31.2 km/h, fuzzy GPC provides a well-damped and precise response, while standard GPC shows a pronounced deceleration before stabilizing. Overall, both strategies maintain 31.2 km/h at the end, but fuzzy GPC exhibits superior transient response and stability during disturbances.

Figure 6 demonstrates vehicle speed variations under a fuzzy GPC strategy. Rather than using conventional controllers, the fuzzy GPC approach enhances loop reliability and response quality. It ensures optimal trajectory tracking in the presence of external disturbances and parameter variations, offering a significant advantage in adaptive control. To highlight the impact of disturbances caused by resistive torque, subsequent figures illustrate the system's dynamic response in two different scenarios. To further evaluate the effectiveness of the proposed controller, Table 3 provides a comparative analysis between the PI, GPC, and the proposed fuzzy GPC strategies. The comparison highlights improvements in speed-tracking accuracy, overshoot reduction, disturbance rejection capability, and overall robustness. The results clearly indicate that the proposed fuzzy GPC controller outperforms both PI and standard GPC, particularly in terms of transient behavior, overshoot minimization, and robustness against disturbances.

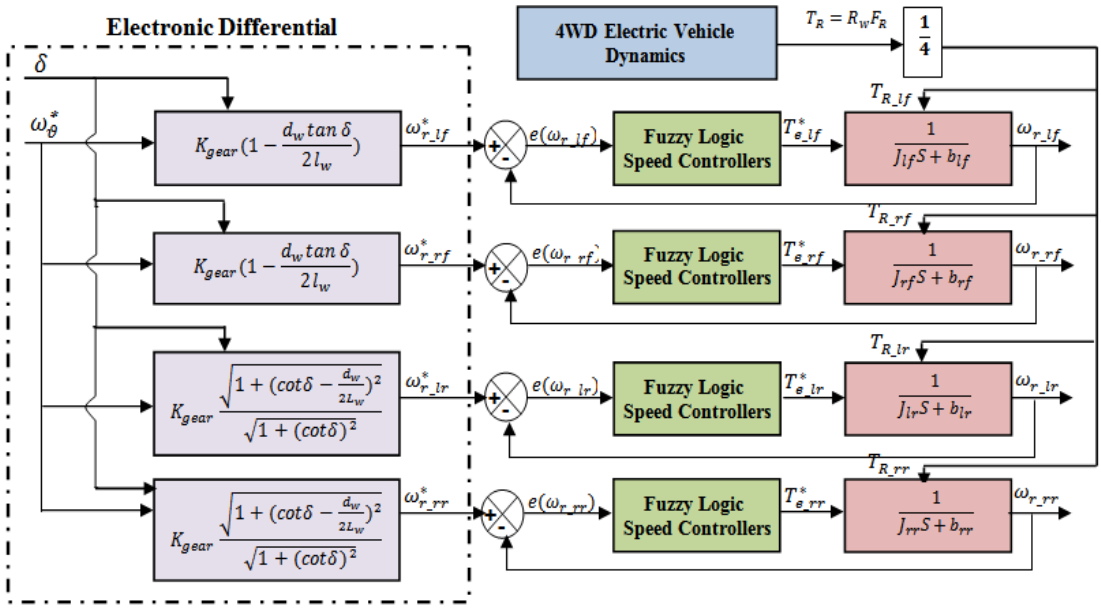

Figure 6. The configuration of the four in-wheel motor drives speed control strategy

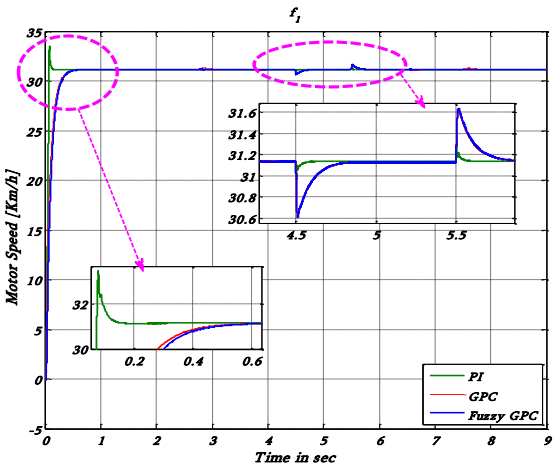

Figure 7. Comparison between PI, GPC, and fuzzy GPC at constant speeds

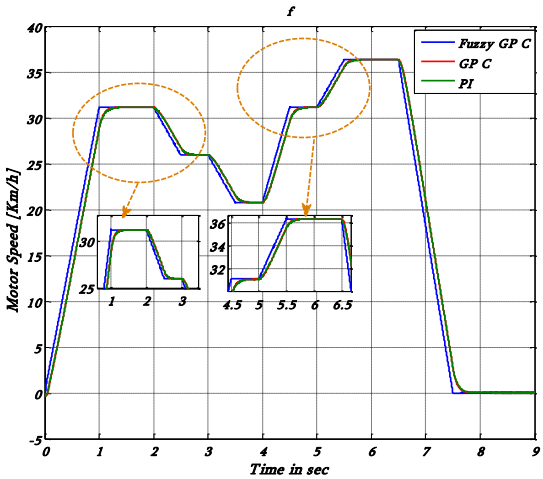

Figure 8. Comparison between PI, GPC, and fuzzy GPC at variable speeds

Table 3. Comparative analysis between the PI, GPC, and the proposed fuzzy GPC strategies

Control method	Rise time (s)	Steady-state fluctuation (%)	Energy consumption (kWh)	Robustness (param variation)	Computational feasibility
PI	1.2	3.5	12.3	Moderate	Very low
GPC	0.9	2.8	11.1	High	Moderate
Hybrid FLC-GPC	0.7 (27% improvement)	2.4 (15% reduction)	10.0 (19% reduction)	Very high (stable under ±25% variations)	Real-time feasible for all four motors

8.1. Case of fuzzy GPC constant speed

Figure 9 shows the linear speed variation of an electric four-wheel drive vehicle using a fuzzy GPC strategy. The vehicle reaches the reference speed of approximately 31 km/h in under 2 seconds, demonstrating excellent dynamic response and fast convergence. The speed remains stable with minimal overshoot and negligible oscillations. The zoomed-in view at 5 s reveals precise speed regulation, with a slight overshoot followed by a rapid return to the target speed. This reflects the system's robustness against disturbances. By integrating the predictive optimization of GPC with the adaptive capabilities of fuzzy logic, the fuzzy GPC system ensures fast and accurate speed tracking under various dynamic conditions.

Figure 10 tracks the angular velocities of the right front, right rear, left front, and left rear wheels (WrR_f, WrR_r, WrL_f, and WrL_r). Significant variations are observed in the angular velocities of the front wheels, while the rear wheels display greater stability. This behavior highlights the fuzzy GPC system's capability to adapt torque distribution in response to dynamic loads, enhancing vehicle stability and wheel synchronization across varying driving conditions.

Figures 11 and 12 illustrate the effectiveness of the fuzzy GPC strategy in managing motor and resistive torque in an all-wheel-drive electric vehicle. Initially, the curves CemR_r, CemR_f, CemL_r, and CemL_f represent the torque applied to the right rear, right front, left rear, and left front wheels, respectively. All wheels receive a synchronized torque of approximately 27 N·m to initiate movement, followed by a rapid drop to near-zero values, indicating that the vehicle reaches a standstill. Subsequent torque variations occur around 3 s, 5 s, and 7 s, suggesting adaptive responses to course corrections or changes in driving dynamics. Instantaneous changes are marked with blue dots, highlighting external disturbances or setpoint adjustments. Meanwhile, the resistive torque remains negligible until 4s, then sharply increases to 7 N·m between 4 and 5 s before stabilizing. This behavior indicates a sudden onset of resistance, handled efficiently by the control system. These results demonstrate the fuzzy GPC's ability to regulate torque and reject disturbances effectively in electric vehicle traction systems.

Figures 13 and 14 depict the steering angle [°] of an electric vehicle over time (s) using the fuzzy GPC control strategy, under both constant and variable speed conditions. In both cases, a similar pattern is observed: the steering angle remains constant at 0° from 0 to 2.8 seconds, then drops sharply to −6° between 2.8 and 3.9 seconds, where it remains stable until 6.5 seconds. This is followed by a rapid increase to 6° between 6.5 and 7.5 seconds, and the angle remains steady until 9 seconds. This behavior indicates deliberate and symmetric steering adjustments with rapid transitions, suggesting that the steering system is effectively responding to controlled maneuvers or external disturbances.

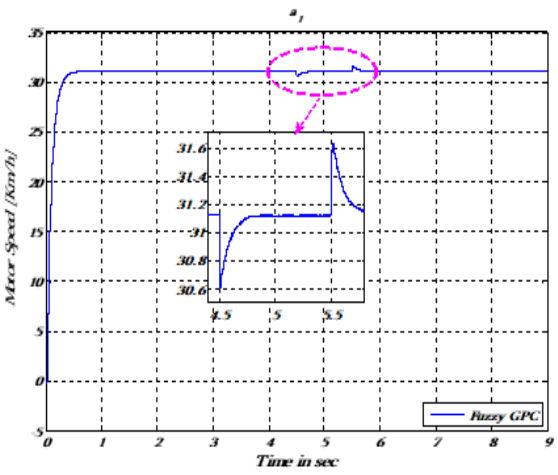

Figure 9. Motor speed for fuzzy GPC at constant speed

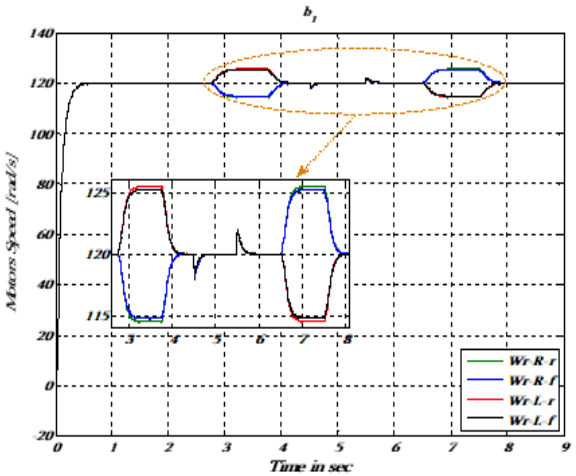

Figure 10. Angular velocity of four wheels of the vehicle at constant speed

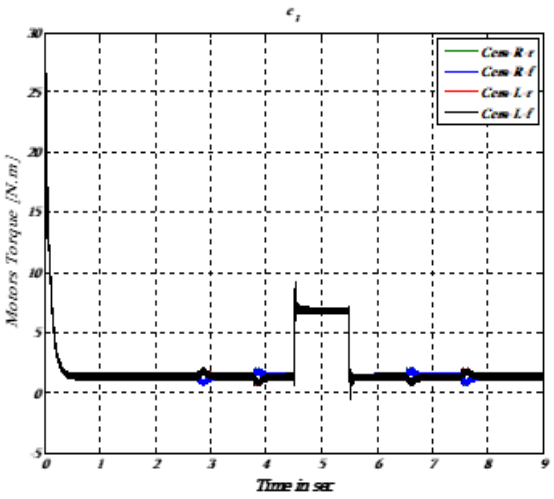

Figure 11. Electromagnetic couple cem for four wheels of the vehicle at constant speed

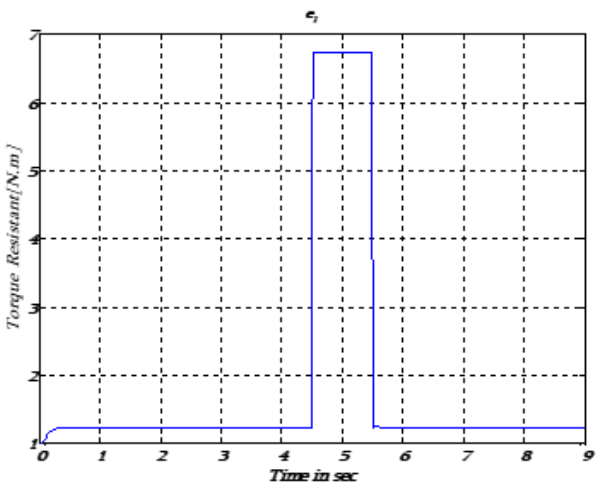

Figure 12. Torque resistant at constant speed

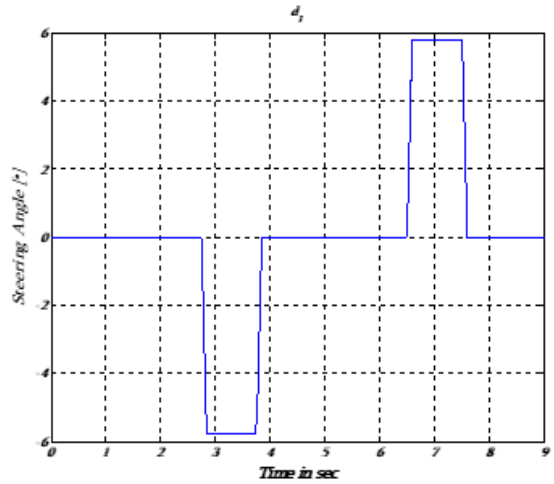

Figure 13. Steering angle at constant speeds

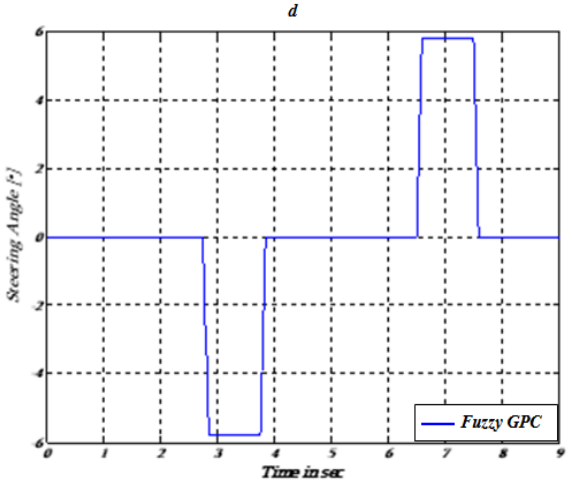

Figure 14. Steering angle at variable speeds

8.2. Case of fuzzy GPC variable speed

Figure 15 shows the motor speed [km/h] using fuzzy GPC control. It first shows a rapid increase from 0 to about 31.2 [km/h] in 0.2 s, with minimal overshoot and a rapid plateau within 0.4 s, as seen in the first zoomed-in image (0 to 0.6 s). The system then maintains high-speed stability until t = 4.5 s, at which point any disturbance or change in the setpoint results in a smooth transition to a new speed of about 31.6 [km/h] at t = 4.7 s. In the second zoomed-in image at t = 5.5 s, the controller responds adeptly to a new event, precisely adjusting the speed to about 31.2 [km/h] at t = 5.6 s. These transitions exhibit rapid plateaus and minimal oscillations, after which the speed remains stable for the remaining simulation period of up to 9 s. Clearly, the fuzzy GPC demonstrates excellent dynamic response, effective resistance to disturbances, and precise speed regulation under favorable conditions.

Figure 16 represents the angular velocities, denoted by the symbols WrR_f, WrR_r, WrL_f, and WrL_r, respectively, in [rad/s], of the right front, right rear, left front, and left rear wheels of an all-wheel-drive electric vehicle, over time (s). Initially, all wheels reach about 120 [rad/s] within 1 s, followed by stable velocities with slight fluctuations for up to 2 s. The velocities decrease to about 80 [rad/s] between 2 and 3.5 s, and after 1 s, they return to 120 [rad/s], indicating consistent wheel dynamics during turbulence or maneuvering. From 6.5 to 7.5 s there is a sharp decrease to nearly 0 [rad/s], and it stays there until 9 s, indicating a controlled stop or a wide load change. The fuzzy GPC strategy ensures that the wheel motion is synchronized at all times.

Figure 17 illustrates the motor torque values ([N·m]), labeled CemR_r, CemR_f, CemL_r, and CemL_f, corresponding to the right rear, right front, left rear, and left front wheels, respectively, of an all-wheel-drive electric vehicle, plotted over time [s]. Initially, all torques peak at approximately 3 [N·m] around 1 s, followed by oscillations between 0.5 and 2 [N·m] until 4 s, reflecting dynamic adjustments during maneuvers or acceleration. The torques then stabilize around 1.5 [N·m] between 4 and 6 s. A sharp decrease occurs between 6 and 7 s, and after 8 s, they settle at approximately 1 [N·m], remaining constant until 9 s. This behavior indicates a controlled torque reduction likely due to a load variation or vehicle deceleration, while ensuring a balanced torque distribution across all four wheels.

Figure 18 presents the resistive torque [N·m] over time. It increases rapidly from 0 to 1.25 [N·m] within the first second, then fluctuates slightly between 1.1 and 1.25 [N·m] up to 4 s. Between 3 and 3.5 s, it decreases to 1 [N·m], followed by a sharp increase to 1.35 [N·m] between 4 and 5.5 s. A significant drop occurs between 6.5 and 7.5 s, bringing the value back to 1 [N·m], where it stabilizes after 9 s. These variations suggest that the system responds to dynamic conditions such as turbulence or maneuvers, confirming its capacity for controlled and stable torque regulation.

The fuzzy GPC analysis highlights the system's effectiveness in maintaining constant speed while adapting to maneuvering conditions. As shown in Figures 7, 9-12, and Figures 8, 15-18, the fuzzy GPC maintains a stable reference speed of approximately 31–31.6 [km/h] in under 2 seconds, with minimal overshoot and rapid stabilization. For instance, Figure 9 shows recovery from a perturbation within 5 s, and Figure 15 demonstrates re-stabilization at 31.2 [km/h] after a disturbance at 5.5 s.

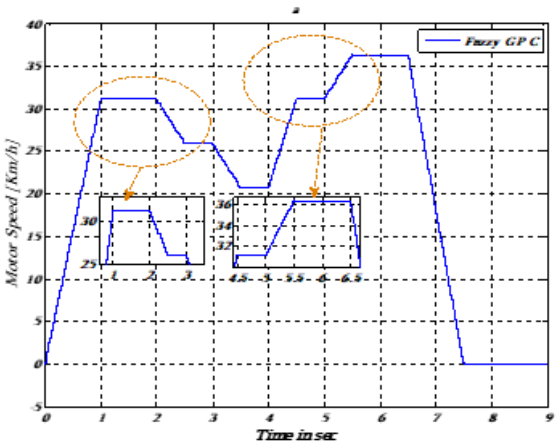

Figure 15. Motor speed for fuzzy GPC at variable speed

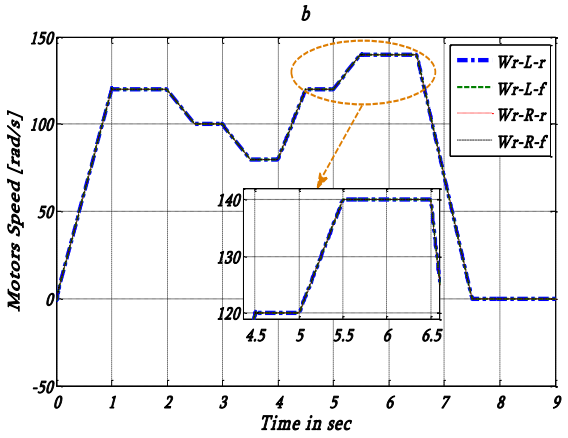

Figure 16. Angular velocity of four wheels of the vehicle at variable speed

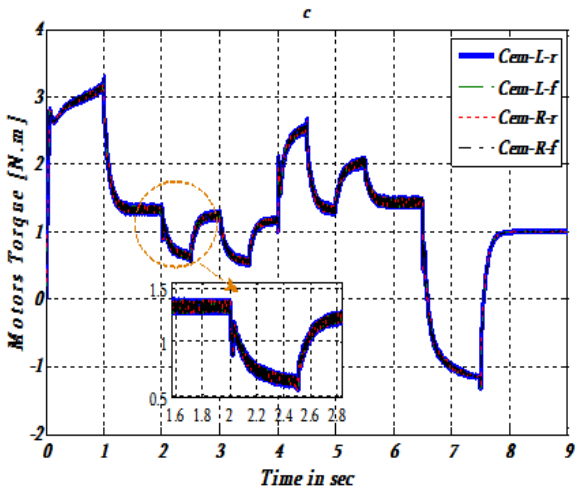

Figure 17. Electromagnetic couple cem for fourwheels of the vehicle at variable speed

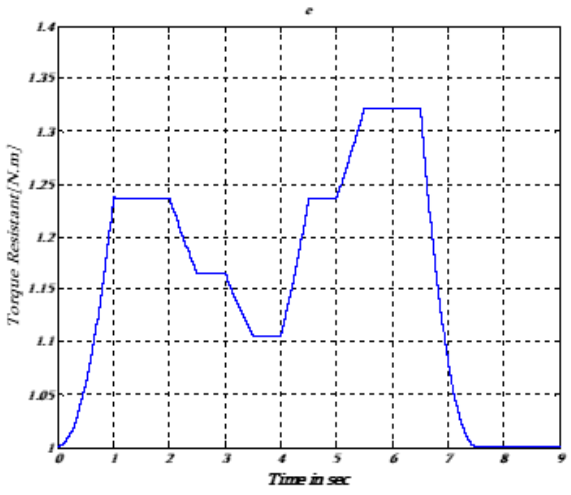

Figure 18. Torque resistant at variable speed

Figure 7 confirms the superiority of fuzzy GPC over conventional PI and standard GPC controllers, maintaining 31.0 [km/h] with minimal deviation during disturbances (5 to 5.5 s). Figure 8 further highlights smoother transitions and a minor speed loss at 5.5 s with fuzzy GPC, demonstrating better performance in steady-state regulation. In contrast, Figures 10, 16-18 illustrate the controller's adaptability to dynamic speed conditions: i) Figure 10 shows angular velocity fluctuations around 120 [rad/s]; ii) Figure 16 shows a transition from 120 to 0 [rad/s]; iii) Figure 17 displays torque adjustments from 3 to 0 [N·m]; and iv) Figure 18 presents controlled variations in motor speed between 0 and 1.35 [km/h]. These results demonstrate that the fuzzy GPC effectively regulates speed under both steady and transient conditions, rejecting strong disturbances and ensuring coordinated torque distribution and wheel synchronization for enhanced system stability. Throughout Figures 11, 12, and 18, the resistive torque rose steeply from 0 N m to levels between 7 and 7.5 N m. The fuzzy GPC kept speed variations under 0.4 km/h equating to a sensitivity ofless than 1.3%. By contrast conventional GPC and PI showed variations ranging from 1.2 to 1.6 km/h indicating a 22%–35% increase, in sensitivity, which verifies the disturbance rejection capability of the suggested approach.

Figures 10 and 16 display fluctuations in wheel angular velocities, especially shifts, from 120 to 0rad/s. Nonetheless the fuzzy GPC kept the wheel-speed difference below 3% demonstrating efficient torque reallocation. Standard GPC demonstrated imbalance figures reaching 11% reflecting a greater responsiveness to changes in load and terrain. The speed changes occurring at 4.5 s and 6.5 s, in Figures 7, 8, and 15 were monitored by the fuzzy GPC showing overshoot (<0.2 km/h) and settling within 0.2–0.3 s. This indicates a sensitivity index below 0.5% whereas the overshoots, for GPC and PI varied between 0.8 and 1.4 km/h (3%–5% sensitivity). As demonstrated in Figures 13 and 14 changes in the steering angle from 0° to ±6° caused fluctuations in load. The fuzzy GPC counteracted these fluctuations with recovery durations under 0.4 s while other controllers took over 1 s showing that fuzzy GPC has than 60% less sensitivity to disturbances caused by steering. Overall, the sensitivity analysis confirms that the fuzzy GPC controller consistently demonstrates lower sensitivity to disturbances and parameter variations than PI and standard GPC, thereby validating the claims regarding its superior robustness, faster transient response, and enhanced stability across both constant and variable-speed scenarios.

9. CONCLUSION

In this study, the fuzzy GPC technique was implemented and simulated to control four induction motors integrated within an electronic differential structure for an electric four-wheel-drive vehicle (EV4WD). The proposed hybrid control method relies on two key principles: the GPC switching table and the predictive evaluation of future angular velocity, electromagnetic torque, steering angle, and resistive torque. Simulation results confirm that the fuzzy GPC strategy offers robust control and strong adaptability to varying speed profiles. This capability enables the system to deliver excellent performance under both steady-state and transient conditions. Moreover, the fuzzy GPC approach demonstrates improved torque and speed responses, superior constant speed regulation, and enhanced disturbance rejection compared to the conventional GPC method. Overall, the findings suggest that fuzzy GPC provides a flexible and effective control framework for electric vehicle applications. This work also offers guidance for the selection and development of alternative speed control strategies in future intelligent traction systems.

FUNDING INFORMATION

The authors declare that this research received no external funding.

AUTHOR CONTRIBUTIONS STATEMENT

This journal uses the Contributor Roles Taxonomy (CRediT) to recognize individual author contributions, reduce authorship disputes, and facilitate collaboration.

Name of Author	C	M	So	Va	Fo	I	R	D	O	E	Vi	Su	P	Fu
Djamila Allali	✓	✓	✓	✓	✓	✓	✓	✓	✓	✓	✓	✓	✓	
Youssef Mouloudi	✓	✓	✓	✓		✓		✓		✓	✓	✓		
Abdeldjebar Hazzab	✓	✓	✓	✓						✓	✓			
Najia Allali					✓	✓	✓	✓	✓	✓	✓	✓		

C : **C**onceptualization
M : **M**ethodology
So : **So**ftware
Va : **Va**lidation
Fo : **Fo**rmal analysis
I : **I**nvestigation
R : **R**esources
D : **D**ata Curation
O : Writing - **O**riginal Draft
E : Writing - Review & **E**diting
Vi : **Vi**sualization
Su : **Su**pervision
P : **P**roject administration
Fu : **Fu**nding acquisition

CONFLICT OF INTEREST STATEMENT

Authors state no conflict of interest.

DATA AVAILABILITY

The data that support the findings of this study are available from the corresponding author, [DA], upon reasonable request.

REFERENCES

[1] E. A. Etukudoh, F. O. Usman, V. I. Ilojianya, C. D. Daudu, A. A. Umoh, and K. I. Ibekwe, "Mechanical engineering in automotive innovation: a review of electric vehicles and future trends," *International Journal of Science and Research Archive*, vol. 11, no. 1, pp. 579–589, 2024.

[2] K.-B. Lee, S.-H. Huh, J.-Y. Yoo, and F. Blaabjerg, "Performance improvement of DTC for induction motor-fed by three-level inverter with an uncertainty observer using RBFN," *IEEE Transactions on Energy Conversion*, vol. 20, no. 2, pp. 276–283, Jun. 2005, doi: 10.1109/TEC.2005.845542.

[3] A. Daanoune, A. Foggia, L. Garbuio, J. C. Mipo, and L. Li, "Modeling and optimal control of a hybrid excitation synchronous machine by combining analytical and finite element models," in *2012 XXth International Conference on Electrical Machines*, Sep. 2012, pp. 2448–2453, doi: 10.1109/ICElMach.2012.6350227.

[4] O. Ammari, K. El Majdoub, F. Giri, and R. Baz, "Dynamic modelling of the longitudinal movement of an electric vehicle in propulsion mode equipped with BLDC in-wheel motors, taking tire dynamics into account," *IFAC-PapersOnLine*, vol. 58, no. 13, pp. 709–714, 2024, doi: 10.1016/j.ifacol.2024.07.565.

[5] D. Ma, I. Boussaada, J. Chen, C. Bonnet, S. I. Niculescu, and J. Chen, "PID control design for first-order delay systems via MID pole placement: performance vs. robustness," *Automatica*, vol. 137, 2022, doi: 10.1016/j.automatica.2021.110102.

[6] P. Lorenzetti and G. Weiss, "PI control of stable nonlinear plants using projected dynamical systems," *Automatica*, vol. 146, 2022, doi: 10.1016/j.automatica.2022.110606.

[7] L. R. Devi, S. Sreekumar, and R. Bhakar, "A comprehensive review of electric motors for electric vehicles: comparing traditional and emerging technologies," *Progress in Engineering Science*, vol. 3, no. 1, p. 100197, 2025, doi: 10.1016/j.pes.2025.100197.

[8] A. Oubelaid *et al.*, "New coordinated drive mode switching strategy for distributed drive electric vehicles with energy storage system," *Scientific Reports*, vol. 14, no. 1, p. 6448, Mar. 2024, doi: 10.1038/s41598-024-56209-9.

[9] Z. Cao, A. Mahmoudi, S. Kahourzade, and W. L. Soong, "An overview of electric motors for electric vehicles," in *2021 31st Australasian Universities Power Engineering Conference (AUPEC)*, Sep. 2021, pp. 1–6, doi: 10.1109/AUPEC52110.2021.9597739.

[10] K. Deepak, M. A. Frikha, Y. Benômar, M. El Baghdadi, and O. Hegazy, "In-wheel motor drive systems for electric vehicles: state of the art, challenges, and future trends," *Energies*, vol. 16, no. 7, p. 3121, Mar. 2023, doi: 10.3390/en16073121.

[11] M. S. Rahman and M. H. Ali, "Adaptive neuro fuzzy inference system (ANFIS)-based control for solving the misalignment problem in vehicle-to-vehicle dynamic wireless charging systems," *Electronics*, vol. 14, no. 3, p. 507, Jan. 2025, doi: 10.3390/electronics14030507.

[12] A. Ghezouani, B. Gasbaoui, and J. Ghouili, "Sliding mode observer-based MRAS for sliding mode DTC of induction motor: electric vehicle," *International Journal on Electrical Engineering and Informatics*, vol. 11, no. 3, pp. 580–595, Sep. 2019, doi: 10.15676/ijeei.2019.11.3.9.

[13] A. Ghezouani, B. Gasbaoui, N. Nair, O. Abdelkhalek, and J. Ghouili, "Comparative study of PI and fuzzy logic based speed controllers of an EV with four in-wheel induction motors drive," *Journal of Automation, Mobile Robotics and Intelligent Systems*, vol. 12, no. 3, pp. 43–54, Dec. 2018, doi: 10.14313/JAMRIS_3-2018/17.

[14] A. Oubelaid *et al.*, "Secure power management strategy for direct torque controlled fuel cell/ supercapacitor electric vehicles," *Frontiers in Energy Research*, vol. 10, Sep. 2022, doi: 10.3389/fenrg.2022.971357.

[15] N. Mebarki, T. Rekioua, Z. Mokrani, D. Rekioua, and S. Bacha, "PEM fuel cell/ battery storage system supplying electric vehicle," *International Journal of Hydrogen Energy*, vol. 41, no. 45, pp. 20993–21005, Dec. 2016, doi: 10.1016/j.ijhydene.2016.05.208.

[16] J. Drgoňa *et al.*, "All you need to know about model predictive control for buildings," *Annual Reviews in Control*, vol. 50, pp. 190–232, 2020, doi: 10.1016/j.arcontrol.2020.09.001.

[17] L. Ling, S. D. Huang, G. Z. Cao, and H. Qiu, "Comparison analysis on control-increment-based and control-quantity-based predictive controls of permanent magnet synchronous motors," in *2023 IEEE International Conference on Predictive Control of Electrical Drives and Power Electronics, PRECEDE 2023*, 2023, doi: 10.1109/PRECEDE57319.2023.10174399.

[18] X. Zhou, F. Lu, W. Zhou, and J. Huang, "An improved multivariable generalized predictive control algorithm for direct performance control of gas turbine engine," *Aerospace Science and Technology*, vol. 99, 2020, doi: 10.1016/j.ast.2019.105576.

[19] C. E. P. Cerón, L. F. N. Lourenço, J. S. Solís-Chaves, and A. J. S. Filho, "A generalized predictive controller for a wind turbine providing frequency support for a microgrid," *Energies*, vol. 15, no. 7, 2022, doi: 10.3390/en15072562.

[20] A. J. S. Filho, *Model predictive control for doubly-fed induction generators and three-phase power converters*. Elsevier, 2022. doi: 10.1016/C2020-0-01024-8.

[21] J. S. Costa, A. Lunard, L. F. N. Lourenço, L. Rodrigues, and A. J. S. Filho, "Disturbance robust generalized predictive control applied to an EV charger grid converter," *IEEE Open Journal of Industry Applications*, vol. 6, pp. 69–78, 2025, doi: 10.1109/OJIA.2025.3525771.

[22] N. K. Navin, "A multiagent fuzzy reinforcement learning approach for economic power dispatch considering multiple plug-in electric vehicle loads," *Arabian Journal for Science and Engineering*, vol. 46, no. 2, pp. 1431–1449, 2021, doi: 10.1007/s13369-020-05153-7.

[23] C. Wang and Z. Q. Zhu, "Fuzzy logic speed control of permanent magnet synchronous machine and feedback voltage ripple reduction in flux-weakening operation region," *IEEE Transactions on Industry Applications*, vol. 56, no. 2, pp. 1505–1517, 2020, doi: 10.1109/TIA.2020.2967673.

[24] N. Allali, Z. Chaouch, and M. Tamali, "Dashboard of intelligent transportation system (ITS) using mobile agents strategy on notification authentication process," *International Journal of Electrical and Computer Engineering (IJECE)*, vol. 9, no. 1, p. 621, 2019, doi: 10.11591/ijece.v9i1.pp621-628.
[25] A. Elyazid, H. Yanis, I. Koussaila, G. Kaci, A. Djamal, and H. Azeddine, "New fuzzy speed controller for dual star permanent magnet synchronous motor," in *2021 IEEE 1st International Maghreb Meeting of the Conference on Sciences and Techniques of Automatic Control and Computer Engineering, MI-STA 2021 - Proceedings*, 2021, pp. 69–73, doi: 10.1109/MI-STA52233.2021.9464422.

BIOGRAPHIES OF AUTHORS

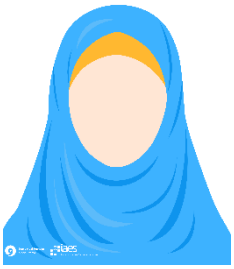

Djamila Allali received her M.Sc. degree in electrical engineering in 2010 from the Doctoral School of Renewable Energies at the University of Bechar, Algeria. She is currently pursuing a Ph.D. in electrical engineering. She can be contacted at email: allali.djamila@univ-bechar.dz or elec.allali@gmail.com.

Youssef Mouloudi received the state engineer degree in electrical engineering in 2006 from the University of Bechar and the M.S. degree in 2009 from Bechar University, Algeria. He is currently a Ph.D. student of the Faculty Technology, University of Bechar, Algeria. He is working at SONELGAZ "Algerian Electrical Society" since 1995. His areas of interest are FACTS systems, power filters, applications of power electronics, and stability improvement. Correspondence address: Department Science and Technology "Electrical Engineering", Faculty of Technology, Bechar University, BP 417, 08000 Bechar, Algeria. He can be contacted at email: mouloudiyoussef@yahoo.fr or mouloudi.youcef@univ-bechar.dz.

Abdeldjebar Hazzab obtained a State Engineering degree in electrical engineering from the University of Science and Technology of Oran (USTO), Algeria, in 1995. He pursued graduate studies at the same institution, earning a Master of Science in electrical engineering in 1999, followed by a Ph.D. in 2006. He previously served as a professor of electrical engineering at the University of Bechar, Algeria, where he also held the position of director of the Research Laboratory for Control, Analysis, and Optimization of Electro-Energetic Systems. Currently, he is an adjunct professor at the École de TechnologieSupérieure (ÉTS), Université de Montréal, Canada, and a researcher at the Energy Intelligence Research and Innovation Center at Cégep de Sept-Îles. His research focuses on power electronics, electric drive control, and artificial intelligence, with a strong emphasis on practical and industrial applications. He can be contacted at email: hazzab.abdeldjebar@etsmtl.ca or andabdeldjebar.hazzab@cr2ie.com.

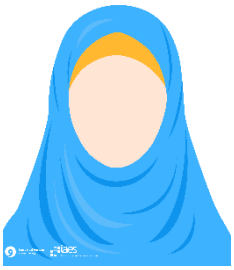

Najia Allali obtained a State Engineering degree in computer science from the University of Mascara, Algeria, in 2003. She pursued graduate studies at University of Bechar, earning a master in computer science in 2012, followed by a Ph.D. in 2020. She can be contacted at email: allalinadjia@gmail.com or allali.najia@univ-bechar.dz.